



Article

Effects of Electron Beam Irradiation on 3D-Printed Biopolymers for Bone Tissue Engineering

Conrad Mastalerz ^{1,*}, Isabelle Vroman ¹, Xavier Coqueret ² and Sébastien Alix ¹

¹ Campus Moulin de la Housse, Université de Reims Champagne-Ardenne, ITheMM EA 7548, 51097 Reims, France; isabelle.vroman@univ-reims.fr (I.V.); sebastien.alix@univ-reims.fr (S.A.)

² Campus Moulin de la Housse, Université de Reims Champagne-Ardenne, CNRS, ICMR UMR 7312, 51097 Reims, France; xavier.coqueret@univ-reims.fr

* Correspondence: conrad.mastalerz@univ-reims.fr

Abstract: Implanting scaffolds designed for the regeneration or the replacement of bone tissue damaged by diseases and injuries requires specially designed biomaterials that promote cell adhesion. However, the biodegradation rate of these scaffolds based on a single material is uniform. Four-dimensional printing appears to be a promising method to control this aspect by changing the shape and/or the intrinsic properties of 3D-printed objects under the influence of external stimuli. Two main classes of biomaterials and biocomposites based on biopolyesters, namely poly(lactic acid) (PLA) and poly(caprolactone) (PCL), were used in this study. Each of them was mixed with the inorganic filler hydroxyapatite (HA), which is a component of natural bone. The biocomposites and biomaterials were prepared using the melt extrusion process and then shaped using a 3D printer. Three-dimensional specimens showed a decrease in elongation at break and breaking strain due to variations of crystallinity. The crystallinity of irradiated samples increased slightly with irradiation and a new crystalline phase was observed in the case of the PLA. Four-dimensional printing of biomaterials using electron radiation shows great promise for bone tissue engineering based on biocomposite scaffolds and other medical applications.

Keywords: 4D-printing; bone-tissue engineering; biocomposites; electron beam irradiation



Citation: Mastalerz, C.; Vroman, I.; Coqueret, X.; Alix, S. Effects of Electron Beam Irradiation on 3D-Printed Biopolymers for Bone Tissue Engineering. *J. Compos. Sci.* **2021**, *5*, 182. <https://doi.org/10.3390/jcs5070182>

Academic Editor:
Francesco Tornabene

Received: 10 June 2021
Accepted: 7 July 2021
Published: 10 July 2021

Publisher's Note: MDPI stays neutral with regard to jurisdictional claims in published maps and institutional affiliations.



Copyright: © 2021 by the authors. Licensee MDPI, Basel, Switzerland. This article is an open access article distributed under the terms and conditions of the Creative Commons Attribution (CC BY) license (<https://creativecommons.org/licenses/by/4.0/>).

1. Introduction

The growing demand for more efficient bone tissue regeneration techniques fosters the development of new biomaterials with improved properties and additional functionalities. These biomaterials must comply with specifications addressing the needs for various properties including mechanical strength, biocompatibility and biodegradability. Made from polymers, ceramics and/or biocomposites prepared from both types of constituents, biomaterials designed for bone regeneration should also promote cell adhesion and cell proliferation. However, polymers exhibit low mechanical properties, and ceramics do not show acceptable degradation rates for implantable devices. That is why, by mixing the two of them, biocomposites take advantage of the benefits of each to potentially yield biomaterials with excellent mechanical and biological properties for bone tissue engineering.

The most common polymers used in implantable devices are polyesters due to their biocompatibility and their potential to control the degradation rate [1]. In tissue engineering, the most studied and used mineral fillers are hydroxyapatite (HA) [2], β -tricalcium phosphate (β -TCP) [3] and bioglasses [4], because they are close to the constituents of the natural bone. Three-dimensional printing seems particularly adapted to the fast fabrication of customized scaffolds for prosthetic and regenerative surgery [5]. In addition, it allows for the printing of complex structures that would not be possible with other manufacturing processes. Four-dimensional printing is an emerging processing method that induces changes in the shape and/or intrinsic properties of 3D-printed objects under the influence of external stimuli [6]. Among the stimuli that could cause the change in

shape, there was heat, which was highlighted by Wei et al. on PLA/benzophenone for shape memory behavior [7]. Using the same shape-changing mechanism, they also worked on composites of PLA and silver-coated carbon nanofibers using an electric field as an actuation method [8]. A solvent could be used eventually to elaborate a new 4D biofabrication strategy in order to print tubes with a diameter as small as that of the smallest blood vessels using hydrogels [9]. The use of irradiation has also been considered by Zolfagharian et al. in a system containing polystyrene/chitosan/carbon black for shape memory behavior [10]. Concerning applications in tissue regeneration, 4D printing incorporates a time factor, which could further revolutionize bone tissue engineering. The biodegradation rate has always been an important parameter for the design of scaffolds in bone regeneration, specially regarding polymers. Indeed, PLA can take more than two years to biodegrade completely [11]. In our approach, the objective is to modulate the biodegradation of the polymer according to the needs of bone filling and in particular for bone regeneration. The use of biocomposites facilitates bone regeneration, but it is necessary to adapt the resorbability of the polymer matrix. Initial approaches have been made to match the biodegradation rate to the desired time [12].

It has been shown that the irradiation of biocomposites could affect the degradation rate through many studies. Rojdev et al. studied the radiation exposure of boron and carbon fibers with epoxy and concluded that degradation occurred in the system and might enhanced aging [13]. Olewnik-Kruszkowska et al., in their work, highlighted the fact that degradation rate of PLA composites was impacted by fillers and ultra-violet (UV) irradiation [14].

The goal of this study was to include in the fabrication process a radiation treatment that would result in a spatially controlled modulation of the rate of biodegradation of 3D-printed polymer-based scaffolds, as a consequence of cross-linking and scission effects that occur in irradiated polymers. In addition, gamma irradiation is also frequently used for sterilizing implants and prosthetic materials in the medical field [11].

In this study, poly(lactic acid) (PLA) and poly(caprolactone) (PCL) were studied as polymer matrices to further elaborate biocomposites with HA at different filler ratios. The purpose of this is to determinate the maximum filler ratio possible in order to study the influence of filler ratio on thermal properties and further mechanical properties. In this work, electron beam irradiation was used as an external stimulus to apply the 4D printing. Then, both polyesters were irradiated to evaluate the thermal, structural, and mechanical properties of the printed scaffolds under the influence of radiation dose.

2. Materials and Methods

2.1. Materials

PLA pellets were purchased from NaturePlast (Iffs, France). Reference PLE005 is an extrusion grade with the following technical characteristics: density 1.26, melt flow index (190 °C, 2.16 kg) 5–9 g/10 min, glass transition temperature around 60 °C, and melting temperature 170–180 °C. PCL powder was purchased from Perstorp (Warrington, UK). The reference Capa™ 6506 was provided with the following commercial characteristics: molar mass 50,000 g/mol, melt flow index (160 °C, 2.16 kg) 5.2–11.3 g/10 min, and melting temperature 58–60 °C. Spray-dried HA powder was provided from Medicoat (Etupes, France) at a granulometry between 45–150 µm, purity of 95%.

2.2. Biocomposites Manufacturing

PLA and PCL pellets were dried for 12 h at 60 and 40 °C, respectively, before processing. Compounds were prepared using melt extrusion process with BX10 extruder from Axon Plastics Machinery ab (Nyvång, Sweden). For PLA/HA, temperature was set from the feeding area to the die at 185/190/190 °C. Extruder screw rotation was maintained at 20 Hz. Concerning PCL/HA, temperature was set from the feeding area to the die at 95/95/95 °C. Extruder screw rotation was maintained at 20 Hz. Biocomposites were then stored in hermetic plastic bags at room temperature.

2.3. Printing Settings

PLA samples were manufactured using a 3D printer by means of the fused filament fabrication (FFF) process with a Raise3D N2 printer (Irvine, CA, USA). Idea Maker software was used to slice different profiles. The printer nozzle diameter was 0.4 mm and stayed the same for all samples to avoid any deviation. Printing temperature was set at 215 °C for the printer nozzle and 60 °C for the printer build platform and maintained throughout the process. Printing parameters such as printing speed were set at 50 mm/s with a layer thickness of 0.2 mm and line width of 0.4 mm.

PCL powder was manufactured in pellet form using the melt extrusion process at 95 °C and then printed using a 3D-printer pellet additive manufacturing (PAM) process with a PAM P-series printer from Pollen AM (Ivry-sur-Seine, France). A modified Cura software (by Pollen AM) was used to slice different profiles. The printer nozzle diameter was 0.4 mm. Printing temperature was set at 120 °C for the printer nozzle and 35 °C for the printer build platform. Printing parameters such as printing speed were set at 40 mm/s (close to 40 mm/s, because with this process, it was the extrusion speed and the material characteristics that determined the printing speed) with a layer thickness of 0.2 mm and 0.4 mm as line width. All samples were 3D printed in tensile test specimen type 5A to comply with the standard ISO 527-2 with a filling rate of 100%. The slicing profile used one outer shell and an alternating fill pattern of $\pm 45^\circ$ for all layers.

Biocomposites were shaped using the PAM process in a porous architecture of two layers with a layer thickness of 0.2 mm and 0.2 mm as the line width, containing pores of 0.4 mm. Printing parameters were adjusted based on the printing parameters of the polymer matrices.

2.4. Tomography

Architectural biomaterials obtained after printing were observed by tomography, which is a non-destructive technique, in order to observe the distribution of filler within the material. Morphological analyses were carried out twice by formulation using RX Solution EasyTom 150 computer-assisted X-ray tomograph. The parameters were set at a voltage of 60 kV, 166 μ A in intensity, and 10 W in power, with 1440 X-ray images at two images per second for a voxel size less than 20 μ m. Data were analyzed with X-Act software and Vg-studio.

2.5. Electron Beam Irradiation

All tensile tests samples were irradiated in passes of 10 or 25 kGy at most, between 10 and 100 kGy, with a 10 MeV electron beam from a pulsed Linac accelerator at an average dose rate of 15 kGy/s (IONISOS, Chaumesnil, France). Irradiated samples were then directly placed after irradiation in hermetic plastic bags and stored at 2 °C.

2.6. Thermal Analysis

The thermogravimetric analysis (TGA) was carried out by using a thermal analyzer TG 209 F3 Tarsus from Netzsch (Germany). TGA allowed us to evaluate the influence of the HA ratio of biocomposites pellets on the thermal degradation temperature, necessary for 3D printing. About 15 mg of the sample was put in a TGA pan and the analysis was performed from 30 to 600 °C with a heating rate of 10 °C/min. Nitrogen gas was used to keep an inert atmosphere at a flow rate of 20 mL/min.

Differential scanning calorimetry (DSC) allowed us to evaluate the influence of the radiation dose on the thermal and structural properties of irradiated tensile tests samples. It was performed using a DSC Q20 from TA Instruments (New Castle, DE, USA). About 10 mg was weighed in an aluminum pan. To maintain inert atmosphere, nitrogen gas was used with a flow rate of 50 mL/min. Samples were first heated from -80 to 200 °C with a heating rate of 10 °C/min to remove thermal history, then cooled down to -80 °C at a cooling rate of 10 °C. Then, the samples were reheated to 200 °C at 10 °C/min. TA Universal Analysis software allowed us to analyze the measurement data.

2.7. Tensile Tests

Tensile tests were conducted at room temperature using an Instron 3366 (Norwood, MA, USA) with a 10 kN load cell. Five specimens were 3D printed for each irradiation dose: 0, 10, 25, 50, 75 and 100 kGy. All samples had at the middle length a thickness of about 1.5 mm and a width of 4 mm. Traction speed was set at 10 mm/min and was kept constant throughout the tensile tests until the sample break. All data were then retreated to determine the Young’s modulus, breaking stress and elongation at break.

All the processes and characterizations of the biocomposites were shown in Figure 1.

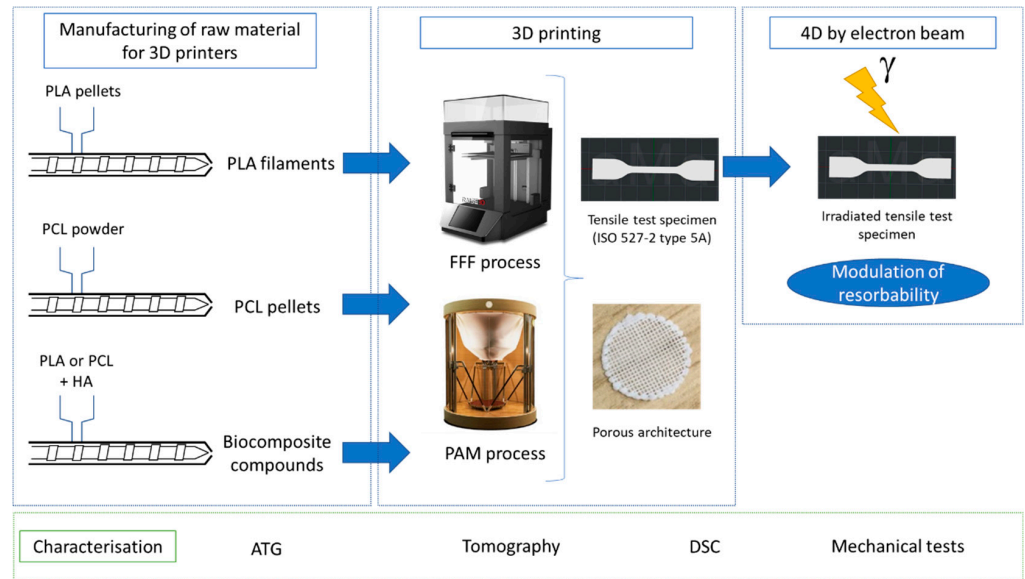


Figure 1. Schematic diagram of the overall experimental section, from materials preparation to characterization tests.

3. Results and Discussions

At first, the influence of radiation treatment with high energy electron beam (EB) was evaluated based on thermal and mechanical properties of unfilled polymer matrices. DSC and tensile analysis were performed. Thus, 3D-printed PLA and PCL were first studied before starting the manufacturing of biocomposites. Then, manufacturing of PLA/HA and PCL/HA were elaborated and analyzed using TGA in order to determine the maximum filler ratio possible and control the amount of filler ratio in each compound produced.

3.1. Thermal Properties

Thermal properties of matrices were analyzed by DSC. Table 1 (PLA) and Table 2 (PCL) report all data from DSC curves from the second heating, including glass transition temperature (T_g), melting temperature (T_m), melting enthalpy (ΔH_m) and degree of crystallinity (X_c).

Table 1. Thermal properties obtained from DSC curves of PLA samples under EB radiation during the second heating.

Doses (kGy)	T_g (°C)	T_{m1} (°C)	T_{m2} (°C)	ΔH_m (J/g)	X_c (%)
0	58.2 ± 0.6	169.8 ± 0.4	176.5 ± 0.3	52.1 ± 0.5	56.0 ± 0.5
10	59.1 ± 1.7	167.3 ± 0.9	174.5 ± 1.5	55.8 ± 4.4	59.9 ± 4.8
25	57.5 ± 3.8	165.8 ± 2.2	172.2 ± 3.1	60.5 ± 6.1	65.1 ± 6.5
50	54.9 ± 1.8	163.0 ± 0.7	169.2 ± 0.7	62.9 ± 1.4	67.6 ± 1.5
75	51.9 ± 0.4	160.4 ± 0.7	166.6 ± 0.7	63.7 ± 0.6	68.5 ± 0.7
100	51.7 ± 0.7	158.6 ± 0.3	165.2 ± 0.3	61.8 ± 1.6	66.4 ± 1.8

Table 2. Thermal properties obtained from DSC curves of PCL samples under EB radiation during the second heating ramp.

Doses (kGy)	T _g (°C)	T _m (°C)	ΔH _m (J/g)	X _c (%)
0	−66.2 ± 0.9	56 ± 0.5	66.3 ± 1.5	48.8 ± 1.1
10	−66.2 ± 0.4	55.9 ± 0.2	65 ± 1.1	47.8 ± 0.8
25	−65.8 ± 1.6	56.5 ± 0.4	66.4 ± 0.5	48.8 ± 0.4
50	−66.7 ± 0.3	55.9 ± 0.2	67 ± 1.4	49.3 ± 1.1
75	−65.7 ± 0.4	55.5 ± 0.1	67.1 ± 0.5	49.3 ± 0.4
100	−64.8 ± 0.4	55.9 ± 0.2	61.6 ± 1.4	45.3 ± 1.1

The thermal history of samples was cleared with the first heating cycle. The first thing that could be observed in the second heating was the effect of irradiations on *T_g*. A regular decrease occurred from 58 to 51 °C for a radiation dose of 100 kGy. This diminution was mostly explained by the diminution of the molecular weight of exposed PLA samples, as shown by Malinowski et al. [15] and Loo et al. [16,17]. Due to changes in chain mobility induced by EB radiation, chain scission brings along greater mobility in macromolecules as the radiation dose increases, resulting in the appearance of *T_g* at a lower temperature. In the case of PCL, *T_g* remained stable, between 65 and 67 °C, indicating that irradiation had little effect on the length of the macromolecular chains of PCL.

The thermograms of the second heating of PLA and PCL are shown in Figures 2 and 3, respectively. The endothermic peaks on thermograms were associated with the melting of each polymer. This second melting peak, in PLA, has put forward a phase transition in the printing process, resulting in a change in crystal structure. Le Marec et al. [18] studied the influence of melt processing conditions on PLA and put forward the formation of α'-form resulting to chain scission that occurred during the process. Only three different crystalline structures were identified in the past for PLA (α, β and γ) depending on the preparation conditions. However, Zhang et al. [19] observed another crystalline form that was close to the α-form and β-form. As in this study, the apparition of the exothermic peak before the melting peak concerned the phase transition of the β-form to a more stable form. Many studies showed and explained that the transition phase [20] leads to a co-existence of crystallites when it is crystallized below 90 °C [21]: α-form and metastable crystalline α'-form, which is called “disordered crystal”.

However, electron radiation had a significant effect on the co-existence of α and α'-form. DSC analysis showed a proportional variation between these crystallites with radiation dose. The proportion of α'-form increased at a higher radiation dose until obtaining an almost identical proportion of α and α'-form. The increase in α'-form in irradiated PLA also influenced melting peaks by decreasing them, starting from 169 and 176 °C, for non-irradiated 3D-printed PLA, to 158 and 165 °C for irradiated PLA at 100 kGy. Since PLA contained less stable form in its crystal structure, specific thermal peaks appeared at lower temperature.

By considering a melting enthalpy of 93 and 136 J/g, respectively for 100% crystalline PLA [22] and PCL [23], crystallinity could be extracted from DSC curves. Irradiations permitted to increase crystallinity of all samples, going from 56% for non-irradiated PLA to 66% for 3D-printed PLA at a radiation dose of 100 kGy. The increase in crystallinity with radiation doses was related to a well-known phenomenon such as chemocrystallization [24] who was also observed on polyhydroxybutyrate [25] and which is quite common in the case of aliphatic polyesters. Indeed, irradiation induced predominant scission reactions that reduce the average length of PLA chains. The whole material gains mobility. This facilitates the reorganization of the polymer chains and induces an increase in the crystallinity.

For PCL samples, as observed in the case of *T_g*, irradiation did not significantly affect the degree of crystallinity for doses up to 75 kGy. Then, a decrease of 4% in crystallinity was observed, which could be the result of an increase in cross-link density in the PCL. This result is in agreement with the observation that PCL chains are less modified at lower radiation dose.

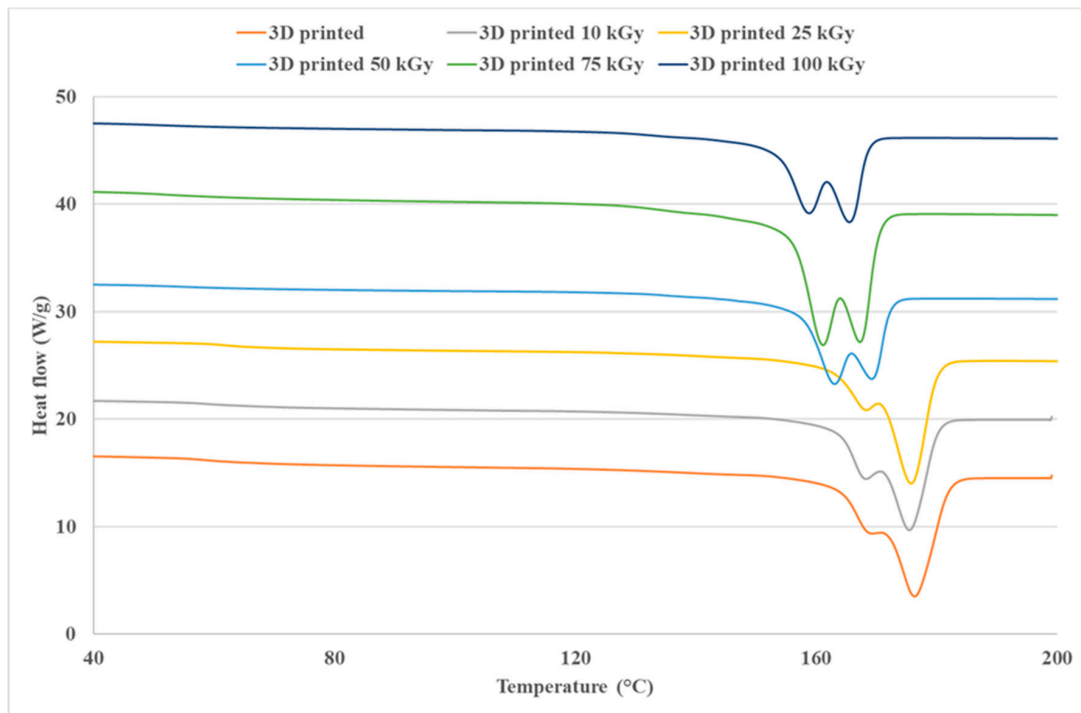


Figure 2. Thermograms of the second heating run of 3D-printed PLA samples after EB treatment at various doses.

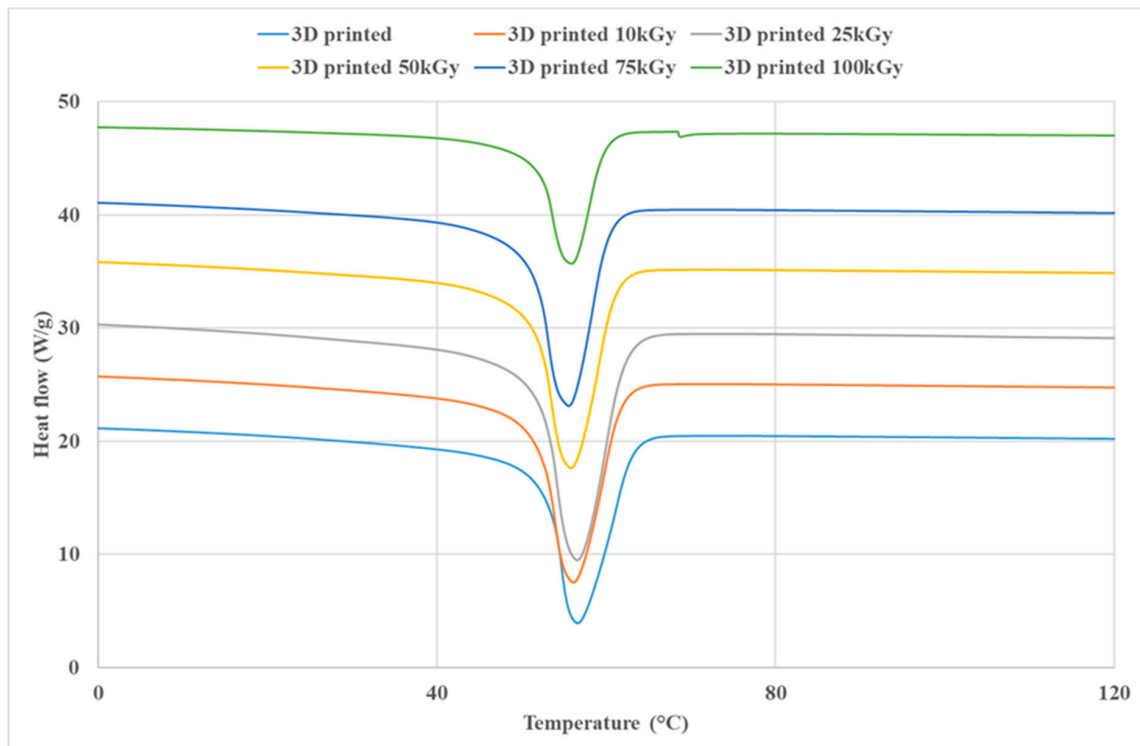


Figure 3. Thermograms of the second heating run of 3D-printed PCL samples after EB treatment at various doses.

3.2. Mechanical Properties

Mechanical properties were analyzed by tensile tests. Results of tensile tests are presented in Figures 4 and 5 for 3D-printed PLA and PCL samples, respectively, as a function of irradiation doses. Considering standard deviations, the Young’s modulus of irradiated and non-irradiated samples varies very little and therefore seems to remain stable. As for PCL, at the highest radiation dose of 100 kGy, an increase up to 200 MPa

could be seen. This increase in stiffness could be explained by a predominant cross-linking effect of the PCL chains, which has already been reported by Malinowski et al. [26].

The tensile stress at break of the printed PLA is around 40 MPa. When the PLA has been irradiated from 10 to 50 kGy, this stress is reduced by 8% (32–34 MPa) but is approximately stable at these doses. After irradiation at 75 and then 100 kGy, the stress at rupture seems to decrease more strongly, especially at 100 kGy, reaching 18 MPa. Regarding elongation at break, the radiation has the effect of decreasing this deformation in a linear manner, ranging from 7% to 2%. These results concur with those presented previously, i.e., with a reduction in the size of the chains and thus a degradation of PLA under irradiation, especially at high doses.

However, non-irradiated printed PCL had a tensile stress at break of 25 MPa and remained stable until a radiation dose of 25 kGy. Higher than this dose, a decrease was seen to reach less than 17 MPa after an irradiation at 100 kGy. Concerning the elongation at break, the tendency followed the same behavior than tensile stress at break. Indeed, the value of elongation at break was close to 1100% until a radiation dose of 25 kGy and was reduced when samples were treated with higher doses, to 500% for 100 kGy. These results are in agreement with the work of Malinowski et al. [26], who found a decrease in tensile stress at break and deformation at break of PCL with triallyl isocyanurate under electron radiation, and are consistent with the hypothesis of PCL cross-linking.

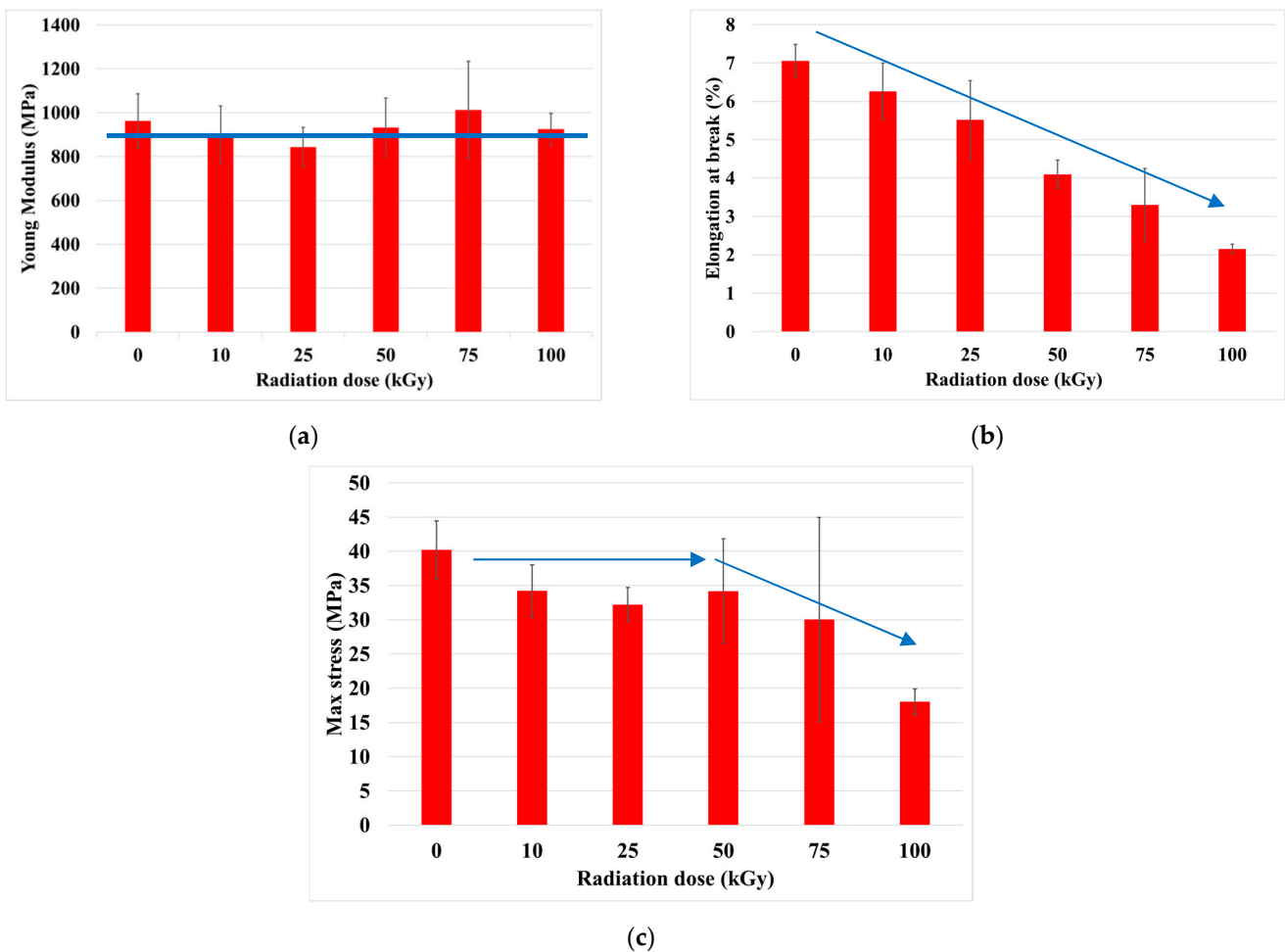


Figure 4. Influence of EB radiation dose on 3D-printed PLA specimens: (a) Young's modulus, (b) elongation at break, (c) max stress.

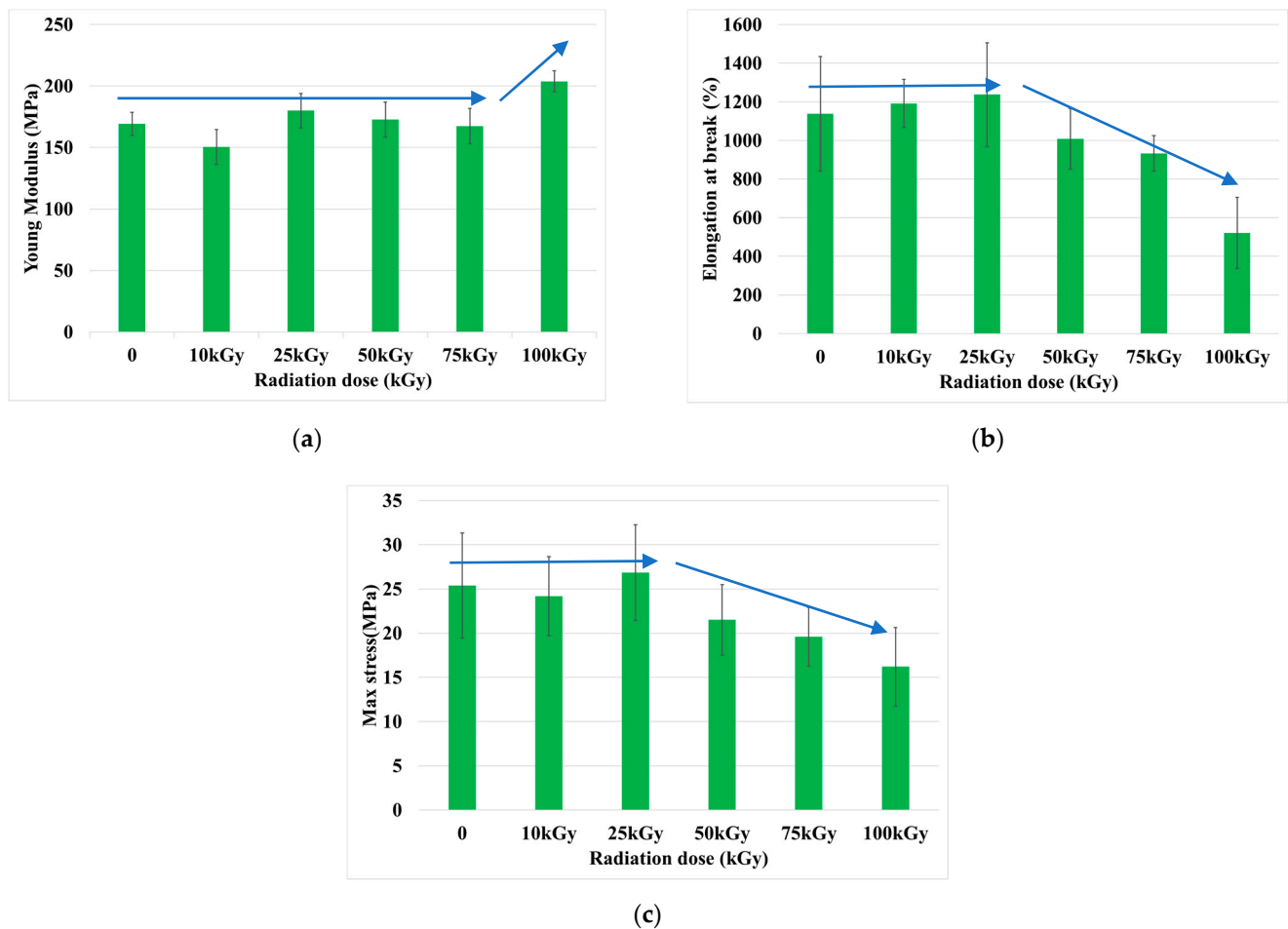


Figure 5. Influence of EB radiation dose on 3D-printed PCL specimens: (a) Young's Modulus, (b) elongation at break, (c) max stress.

Therefore, electron radiations enabled the materials to maintain their elastic properties, but, on the other hand, the plastic properties greatly decreased at higher radiation doses. These effects were highlighted by Madera-Santana et al. [27] and West et al. [28] under gamma radiation on PLA. Chain scissions and oxidative degradation were the main reactions that occurred under irradiation, which implied a diminution of molecular weight by forming shorter chains and/or structures.

However, the lack of deterioration of mechanical properties on PCL under a low radiation dose could be the result of two competitive reactions, cross-linking and chain scission, at the same time. At a lower radiation dose, Darwis et al. [29] explained that cross-linking is predominant in PCL under gamma radiation up to 160 kGy, leading to an increase in mechanical properties. These results are in agreement with the study on PCL and silk fibroin fiber/PCL under EB irradiation from Li et al. [30] and Navarro et al. [31] in their work on PCL of different molecular weights.

Processing polymers with high energy radiation is known to induce modifications of macromolecular structure by competitive chain scission and cross-linking [32]. Results have shown that irradiation has an impact on the crystallinity and structure of polymers, which could affect the biodegradation rate [33]. However, depending on the radiation dose, the effects could be less visible, especially at lower radiation dose. PLA was mostly affected by irradiation, and the same phenomenon was observed in the work of Malinowski et al. [15], although this study put forward the crystal structural change upon irradiation.

Competition between chain scission and cross-linking occurred under irradiation, but, according to the radiation dose, one reaction can be predominant compared to the other. Darwis et al. [29] highlighted this phenomenon in the case of PCL, where it could be seen

in mechanical properties, although our study was carried out in a small range of radiation doses compared to Darwis et al., where they studied a radiation dose of up to 600 kGy. However, γ -radiation and EB-radiation were used in bone tissue engineering specially for sterilization. The radiation dose necessary for sterilization was set at between 25 and 50 kGy and, similarly to the work of Bosworth et al. [34], the sterilization radiation dose was maintained throughout the study.

3.3. Thermogravimetric Analysis of Biocomposites

Pellets of biocomposites (PLA/HA and PCL/HA) were shaped by the melting extrusion process. Biocomposites of PLA/HA and PCL/HA were extruded with a filler ratio up to 60% and 70% (*w/w*), respectively. In order to control the amount of filler, TGA were performed on three pellets of each matrix. Residual mass determined the experimental filler ratio of HA. The results, reported in Figure 6, show that the experimental filler ratio was more accurate in the case of PCL biocomposites due to the mixture of powders, compared to PLA, which is a mixture of pellets and powder. This fact was observed because the mixing of the polymer/fillers was completed before incorporation into the extruder.

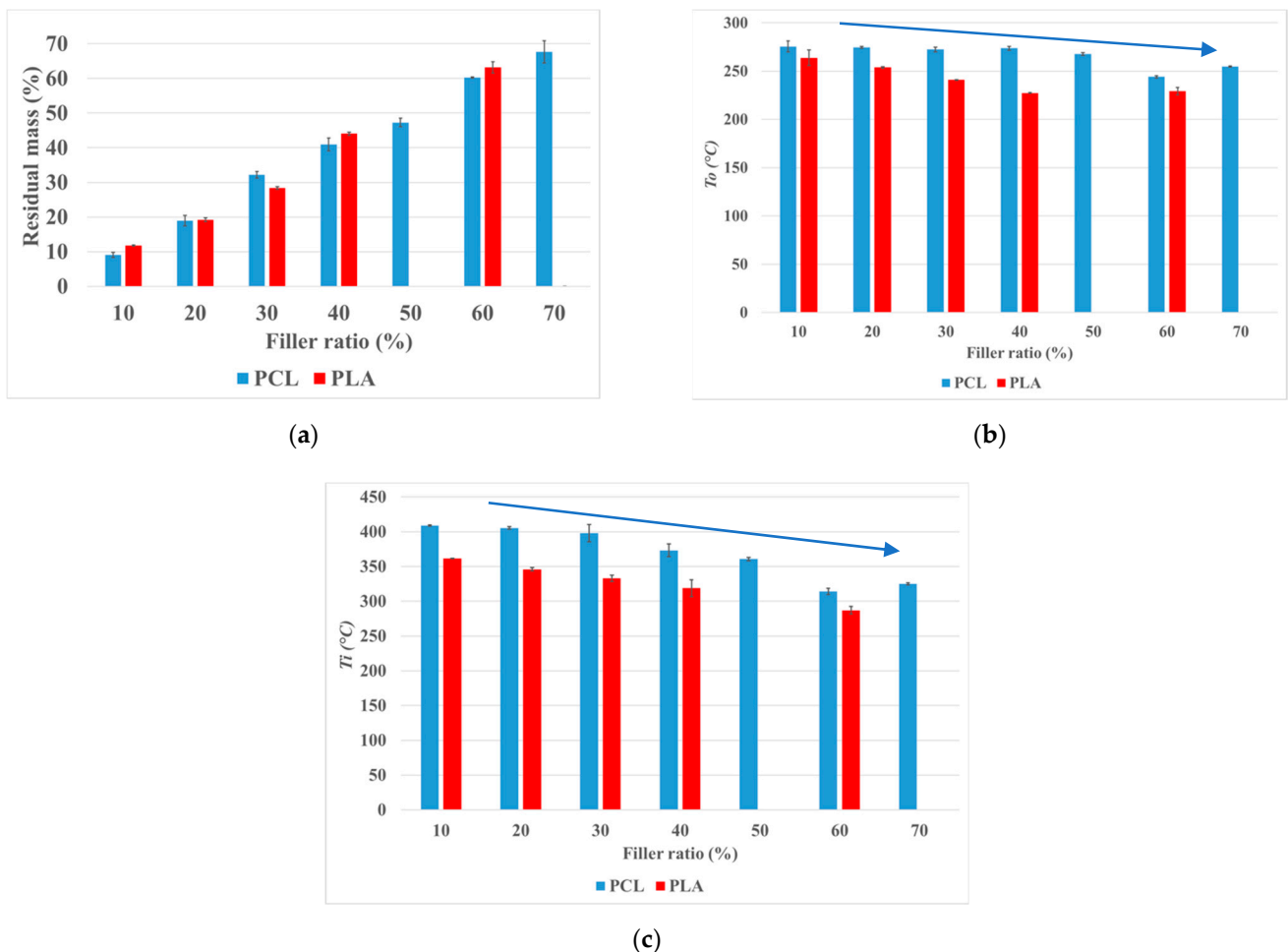


Figure 6. (a) Evaluation of mass residual in biocomposites. (b) Influence of ratio filler dose on the onset thermal degradation temperature T_0 . (c) Influence of ratio filler on the temperature of the inflection point of the degradation curve T_i .

In addition, the onset of the thermal degradation temperature (T_0) was noted when 1% mass loss was seen and the temperature at the inflection point of the degradation curve (T_i) was at the maximum peak of the derivative form of TGA analysis. A linear decrease in the specific degradation temperature with the amount of HA was observed, with a loss of 20 and 34 °C at the maximum filler ratio in T_0 for PCL and PLA, respectively. In the case

of T_i , the results show a diminution of 83 and 74 °C for PCL and PLA, respectively. This effect was explained by the less stable structures of polymer matrices within the composites with the highest amount of ceramics, which induced this decrease in thermal properties. This trend was in agreement with the work of Akindoyo et al. [35] regarding PLA and its composites, with HA at 10% and Biomax® Strong 120.

3.4. Morphological Analysis of Biocomposites

Biocomposites of PLA/HA (20%) and PCL/HA (20%) were manufactured in porous architecture and the filler distribution can be observed in the material in Figure 7. HA particles are marked in green due to their higher density than PCL and PLA, which are accentuated in blue.

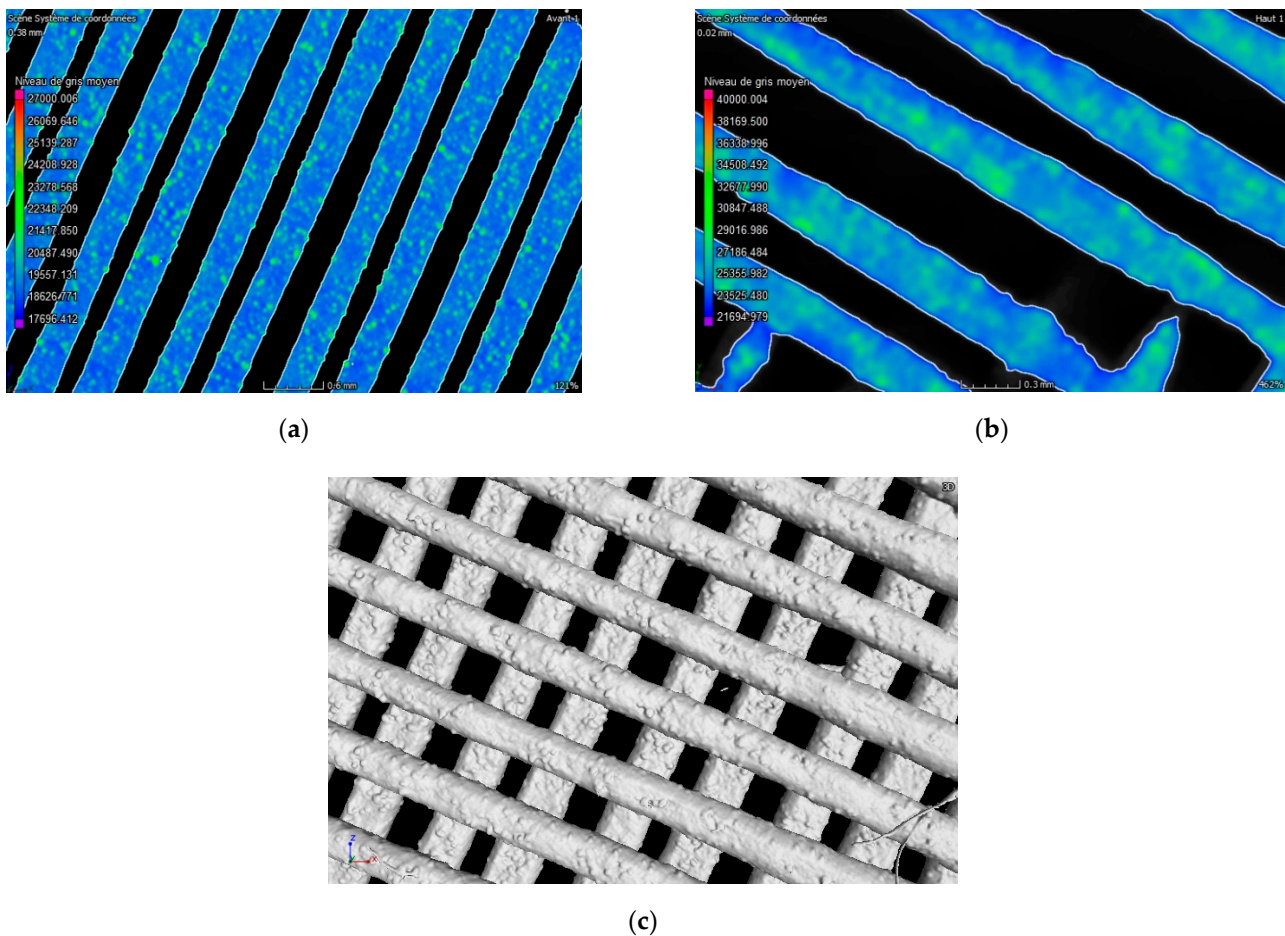


Figure 7. Evaluation of filler distribution in porous architecture of PCL/HA (20%) (a), PLA/HA (20%) (b), external view of porous architecture of PCL/HA (20%).

Fillers of HA presented a great distribution within the printed porous architecture. HA particles were not agglomerated in the center of the filament nor on the ends during the printing process. With the HA particles being well distributed, the mechanical and biological properties induced by the addition of fillers can be observed accordingly for the whole architecture. Furthermore, Figure 7a shows a roughness due to the presence of HA fillers which may be a positive point for cell adhesion in the bone reconstruction process [36].

4. Conclusions

In the case of PLA, the effects of EB radiation were revealed by thermal properties such as the glass transition temperature, which decreased with the dose due to predominant

chain scissions that reduced the average chain length and induced higher chain mobility. Chemicrystallization was observed after the irradiation of PLA samples, with a significant enhancement of the degree of crystallinity. Moreover, the appearance of a second melting peak led to different crystalline structure in PLA, such as α and α' -form, where the proportion of the α' -form increased with the dose of absorbed radiation. This resulted in a loss of the mechanical properties by decreasing the maximum stress and elongation at break because of the shorter length of the PLA chains.

Regarding PCL, the effects of EB radiation were less visible because of the fewer chain scissions and more cross-linking processes that occurred in the polymer at the same time. The deterioration of mechanical properties was observed at a higher radiation dose when chain scission started to be predominant.

Concerning the manufacturing of biocomposites, a high filler ratio decreased the thermal degradation properties due to the less stable structures of polymer matrices. However, it was possible to produce biocomposites with a filler ratio of HA up to 70% (*w/w*), which can be 3D-printed afterward for bone-tissue engineering with a great distribution of HA particles.

Based on the positive results presented in this preliminary report, progress is still being made in the design of 4D-printed biopolymers by means of post-treatment with EB radiation. Studies on the dose-dependance of the biodegradation rate in irradiated biocomposite samples is underway. Scaffolds exhibiting a spatially controlled modulation of polymer structures and properties will be prepared by combining a selection of appropriate materials, printing parameters and post-fabrication irradiation.

In view of this work, the impact of irradiation on biocomposites should be studied. In addition, the application in tissue engineering requires biocompatibility and resorbability tests of biomaterials.

Author Contributions: Conceptualization, S.A., I.V. and X.C.; methodology, C.M.; validation, C.M., S.A., I.V. and X.C.; data curation, C.M.; writing—original draft preparation, C.M.; writing—review and editing, S.A., I.V. and X.C.; supervision, S.A. and I.V.; funding acquisition, S.A. and I.V. All authors have read and agreed to the published version of the manuscript.

Funding: This work is included in the SantePolym4D project and more broadly in the large MIPPI-4D project. This research was co-funded by the Grand Reims (grant number 2018-22) and by the MATUR Chair (grant number F2i 13-2015), co-financed by the Région Champagne-Ardenne (France), the European Union and UIMM. This part of MIPPI-4D project is funded by the Région Grand-Est (France, grant number 18CP-1315).

Conflicts of Interest: The authors declare no conflict of interest.

References

1. Gunatillake, P.; Mayadunne, R.; Adhikari, R. Recent developments in biodegradable synthetic polymers. *Biotechnol. Annu. Rev.* **2006**, *12*, 301–347. [[CrossRef](#)]
2. Granito, R.N.; Renno, A.C.M.; Yamamura, H.; De Almeida, M.C.; Ruiz, P.L.M.; Ribeiro, D.A. Hydroxyapatite from Fish for Bone Tissue Engineering: A Promising Approach. *Int. J. Mol. Cell. Med.* **2018**, *7*, 80–90. [[CrossRef](#)] [[PubMed](#)]
3. Zijderveld, S.A.; Zerbo, I.R.; van den Bergh, J.P.A.; Schulten, E.A.J.M.; ten Bruggenkate, C.M. Maxillary sinus floor augmentation using a beta-tricalcium phosphate (Cerasorb) alone compared to autogenous bone grafts. *Int. J. Oral. Maxillofac. Implant.* **2005**, *20*, 432–440.
4. Hench, L.L. Bioceramics: From Concept to Clinic. *J. Am. Ceram. Soc.* **1991**, *74*, 1487–1510. [[CrossRef](#)]
5. Grémare, A.; Guduric, V.; Bareille, R.; Heroguez, V.; Latour, S.; L'heureux, N.; Fricain, J.-C.; Catros, S.; LeNihouannen, D. Characterization of printed PLA scaffolds for bone tissue engineering. *Biomed. Mater. Res. Part A* **2018**, *106*, 887–894. [[CrossRef](#)] [[PubMed](#)]
6. Miao, S.; Castro, N.; Nowicki, M.; Xia, L.; Cui, H.; Zhou, X.; Zhang, L. 4D printing of polymeric materials for tissue and organ regeneration. *Mater. Today* **2017**, *20*, 577–591. [[CrossRef](#)] [[PubMed](#)]
7. Wei, H.; Zhang, Q.; Yao, Y.; Liu, L.; Liu, Y.; Leng, J. Direct-Write Fabrication of 4D Active Shape-Changing Structures Based on a Shape Memory Polymer and Its Nanocomposite. *ACS Appl. Mater. Interfaces* **2017**, *9*, 876–883. [[CrossRef](#)] [[PubMed](#)]
8. Wei, H.; Cauchy, X.; Navas, I.O.; Abderrafai, Y.; Chizari, K.; Sundararaj, U.; Liu, Y.; Leng, J.; Therriault, D. Direct 3D Printing of Hybrid Nanofiber-Based Nanocomposites for Highly Conductive and Shape Memory Applications. *ACS Appl. Mater. Interfaces* **2019**, *11*, 24523. [[CrossRef](#)] [[PubMed](#)]

9. Kirillova, A.; Maxson, R.; Stoychev, G.; Gomillion, C.; Ionov, L. 4D Biofabrication Using Shape-Morphing Hydrogels. *Adv. Mater.* **2017**, *29*, 1703443. [[CrossRef](#)] [[PubMed](#)]
10. Zolfagharian, A.; Kouzani, A.Z.; Nasri-Nasrabadi, B.; Adams, S.; Khoo, S.Y.; Norton, M.; Gibson, I.; Kaynak, A. In Proceedings of the 2017 International Conference on Design and Technology, Knowledge E, Dubai, United Arab Emirates, 9 February 2017; pp. 15–21. Available online: <https://knepublishing.com/index.php/KnE-Engineering/issue/view/43> (accessed on 10 July 2021).
11. Ikada, Y.; Tsuji, H. Biodegradable polyesters for medical and ecological applications. *Macromol. Rapid Commun.* **2000**, *21*, 117–132. [[CrossRef](#)]
12. Morrison, R.J.; Hollister, S.J.; Niedner, M.F.; Mahani, M.G.; Park, A.H.; Mehta, D.K.; Ohye, R.G.; Green, G.E. Mitigation of tracheo-bronchomalacia with 3D-printed personalized medical devices in pediatric patients. *Sci. Transl. Med.* **2015**, *29*, 7.
13. Rojdev, K.; O'Rourke, M.J.E.; Hille, C.; Nutt, S.; Atwell, W. Radiation effects on composites for long-duration lunar habitats. *J. Compos. Mater.* **2014**, *48*, 861–878. [[CrossRef](#)]
14. Olewnik-Kruszkowska, E.; Koter, I.; Skopińska-Wiśniewska, J.; Richert, J. Degradation of polylactide composites under UV irradiation at 254 nm. *J. Photochem. Photobiol. A Chem.* **2015**, *311*, 144–153. [[CrossRef](#)]
15. Malinowski, R.; Rytlewski, P.; Żenkiewicz, M. Effects of electron radiation on properties of PLA. *Arch. Mater. Sci. Eng.* **2011**, *49*, 25–32.
16. Loo, J.; Ooi, C.; Boey, F. Degradation of poly(lactide-co-glycolide) (PLGA) and poly(l-lactide) (PLLA) by electron beam radiation. *Biomaterials* **2005**, *26*, 1359–1367. [[CrossRef](#)] [[PubMed](#)]
17. Loo, J.; Ooi, C.P.; Boey, Y.C.F. Radiation effects on poly(lactide-co-glycolide) (PLGA) and poly(l-lactide) (PLLA). *Polym. Degrad. Stab.* **2004**, *83*, 259–265. [[CrossRef](#)]
18. Le Marec, P.; Ferry, L.; Quantin, J.-C.; Bénézet, J.-C.; Bonfils, F.; Guilbert, S.; Bergeret, A. Influence of melt processing conditions on poly(lactic acid) degradation: Molar mass distribution and crystallization. *Polym. Degrad. Stab.* **2014**, *110*, 353–363. [[CrossRef](#)]
19. Zhang, J.; Duan, Y.; Sato, H.; Tsuji, H.; Noda, I.; Yan, S.; Ozaki, Y. Crystal Modifications and Thermal Behavior of Poly(l-lactic acid) Revealed by Infrared Spectroscopy. *Macromolecules* **2005**, *38*, 8012–8021. [[CrossRef](#)]
20. Senatov, F.; Zadorozhnyy, M.; Niaza, K.; Medvedev, V.; Kaloshkin, S.; Anisimova, N.; Kiselevskiy, M.; Yang, K.-C. Shape memory effect in 3D-printed scaffolds for self-fitting implants. *Eur. Polym. J.* **2017**, *93*, 222–231. [[CrossRef](#)]
21. Kawai, T.; Rahman, N.; Matsuba, G.; Nishida, K.; Kanaya, T.; Nakano, M.; Okamoto, H.; Kawada, J.; Usuki, A.; Honma, N.; et al. Matsud, Crystallization and Melting Behavior of Poly (l-lactic Acid). *Macromolecules* **2007**, *40*, 9463–9469. [[CrossRef](#)]
22. Davachi, S.M.; Kaffashi, B. Preparation and Characterization of Poly L-Lactide/Triclosan Nanoparticles for Specific Anti-bacterial and Medical Applications. *Polym. Biomater.* **2015**, *64*, 497–508. [[CrossRef](#)]
23. Woodruff, M.A.; Hutmacher, D.W. The return of a forgotten polymer—Polycaprolactone in the 21st century. *Prog. Polym. Sci.* **2010**, *35*, 1217–1256. [[CrossRef](#)]
24. Zaidi, L.; Bruzaud, S.; Kaci, M.; Bourmaud, A.; Gautier, N.; Grohens, Y. The effects of gamma irradiation on the morphology and properties of polylactide/Cloisite 30B nanocomposites. *Polym. Degrad. Stab.* **2013**, *98*, 348–355. [[CrossRef](#)]
25. Oliveira, L.M.; Araujo, E.S.; Guedes, S.M.L. The Effect of Gamma Radiation on Mechanical Properties of Biodegradable Poly-mers poly(3-hydroxybutyrate) and poly(3-hydroxybutyrate-co-3-hydroxyvalerate). *Polym. Degrad. Stab.* **2006**, *91*, 2157–2162. [[CrossRef](#)]
26. Malinowski, R.; Rytlewski, P.; Janczak, K.; Raszewska-Kaczor, A.; Moraczewski, K.; Stepczyńska, M.; Żuk, T. Studies on functional properties of PCL films modified by electron radiation and TAIC additive. *Polym. Test.* **2015**, *48*, 169–174. [[CrossRef](#)]
27. Madera-Santana, T.J.; Meléndrez, R.; González-García, G.; Quintana-Owen, P.; Pillai, S.D. Effect of gamma irradiation on physicochemical properties of commercial poly(lactic acid) clamshell for food packaging. *Radiat. Phys. Chem.* **2016**, *123*, 6–13. [[CrossRef](#)]
28. West, C.; McTaggart, R.; Letcher, T.; Raynie, D.; Roy, R. Effects of Gamma Irradiation upon the Mechanical and Chemical Properties of 3D-Printed Samples of Polylactic Acid. *J. Manuf. Sci. Eng.* **2019**, *141*, 1–21. [[CrossRef](#)]
29. Darwis, D.; Mitomo, H.; Enjoji, T.; Yoshii, F.; Makuuchi, K. Heat resistance of radiation crosslinked poly(ϵ -caprolactone). *J. Appl. Polym. Sci.* **1998**, *68*, 581. [[CrossRef](#)]
30. Li, W.; Qiao, X.; Sun, K.; Chen, X. Effect of Electron Beam Irradiation on the Silk Fibroin Fiber/Poly(ϵ -caprolactone) Composite. *J. Appl. Polym. Sci.* **2009**, *113*, 1063–1069. [[CrossRef](#)]
31. Navarro, R.; Burillo, G.; Adem, E.; Marcos-Fernandez, A. Effect of Ionizing Radiation on the Chemical Structure and the Physical Properties of Polycaprolactones of Different Molecular Weight. *Polymers* **2018**, *10*, 397. [[CrossRef](#)] [[PubMed](#)]
32. Filipczak, K.; Wozniak, M.; Ulanski, P.; Olah, L.; Przybytniak, G.; Olkowski, R.M.; Lewandowska-Szumiel, M.; Rosiak, J.M. Poly(ϵ -caprolactone) biomaterial sterilized by E-beam irradiation. *Macromol. Biosci.* **2006**, *4*, 261–273. [[CrossRef](#)]
33. Roberto, P.; Andrea, S. Influence of crystallinity on the biodegradation rate of injection-moulded poly(lactic acid) samples in controlled composting conditions. *Polym. Degrad. Stab.* **2013**, *98*, 1089–1096.
34. Bosworth, L.A.; Gibb, A.P.; Downes, S.M. Gamma irradiation of electrospun poly(ϵ -caprolactone) fibers affects material properties but not cell response. *J. Polym. Sci. Part B Polym. Phys.* **2012**, *50*, 870–876. [[CrossRef](#)]
35. Akindoyo, J.; Beg, M.; Ghazali, S.; Heim, H.; Feldmann, M. Impact modified PLA-hydroxyapatite composites—Thermo-mechanical properties. *Compos. Part A Appl. Sci. Manuf.* **2018**, *107*, 326–333. [[CrossRef](#)]
36. Martínez-Moreno, D.; Jiménez, G.; Chocarro-Wrona, C.; Carrillo, E.; Montañez, E.; Galocha-León, C.; Clares-Naveros, B.; Gálvez-Martín, P.; Rus, G.; de Vicente, J.; et al. Pore geometry influences growth and cell adhesion of infrapatellar mesenchymal stem cells in biofabricated 3D thermoplastic scaffolds useful for cartilage tissue engineering. *Mater. Sci. Eng. C* **2021**, *122*, 111933. [[CrossRef](#)] [[PubMed](#)]